NASA TECHNICAL
MEMORANDUM

NASA TM X-62,006

NASA TM X-62,006

5–μm LASER RADIATION FROM A CARBON MONOXIDE GASDYNAMIC EXPANSION

by Robert L. McKenzie
Ames Research Center
Moffett Field, Calif. 94035
October 1970

5-μm LASER RADIATION FROM A CARBON MONOXIDE GASDYNAMIC EXPANSION

Robert L. McKenzie

Ames Research Center

SUMMARY

Laser power at 5 μm has been obtained from the gasdynamic expansion of admixtures of carbon monoxide. Mixtures of CO and N_2, diluted in some cases with argon, were heated by reflected shock waves and expanded through a supersonic nozzle containing an optically resonant cavity. The resulting laser radiation, at wavelengths between 4.78 and 5.4 μm, originated from a multitude of partially inverted CO vibrational states. The spectral and laser power characteristics were consistent with radiative gain predictions from numerical solutions of the master rate equations for the vibrational relaxation of anharmonic oscillators. The experimental ratio of multimode laser power, normalized by the total enthalpy flow rate or power supplied to the reservoir, was equal to or greater than that obtained from similar CO_2 gasdynamic lasers.

INTRODUCTION

Although the vibrational relaxation of diatomic molecules has been studied for many years, only recent analyses have brought to light the effects of some important molecular details that can significantly influence the relaxation process. For example, in the past, most theoretical studies assumed an oscillator model containing evenly spaced (harmonic) vibrational quantum states and used the corresponding Landau-Teller[1] transition probabilities in master equations describing their rate of vibrational relaxation. The results led to a relaxation process that proceeded from initial thermal equilibrium through a continuous series of Boltzmann population distributions, often described by a changing vibrational temperature. Analyses based on those assumptions provide useful results when the behavior of only the lowest, nearly harmonic, vibrational levels are of interest. For example, harmonic oscillator models have been applied to CO_2 gasdynamic expansions in which population inversions between the lowest excited vibrational states of the CO_2 asymmetric and symmetric stretch modes were predicted.[2,3] Recently, Treanor et al.[4] showed the small uneven or anharmonic spacing of vibrational energy states occurring in most molecules to cause the upper level nonequilibrium population distributions to become non-Boltzmann, particularly in thermodynamic circumstances where the exchange of vibrational energy between oscillators is a dominant energy transfer mechanism. In the case of rapidly expanding flows from a reservoir in thermal equilibrium, the relaxation of oscillators in each anharmonic vibrational state occurs at a rate that

depends, in part, on the energy spacing and results in an overpopulation of the upper states. For extreme cases, a net inversion may occur.

The overpopulation of upper states, occurring in nonequilibrium thermal expansions of anharmonic diatomic gases, is the physical principle on which the CO gasdynamic laser described in this paper depends. Other CO lasers have been reported previously in which nonequilibrium vibrational excitation is obtained from electric discharges[5-7] or chemical reactions.[8] The power available from discharge or chemical lasers is limited by the size of the discharge or reaction zone and the rate at which molecules in the lower laser states can be removed or re-excited. Similar limitations are present in gasdynamic lasers, but they are less restrictive. Thermally induced inversions can be generated in large volumes by using large or cascaded nozzles and require only that the nozzle reservoir be heated to thermal equilibrium. Moreover, the expended species in the lower laser states are rapidly removed from the laser cavity by the supersonic flow. The available gasdynamic laser power then depends mainly on the mass-flow rate of heated gases that can be provided from any of a variety of energy sources. The power levels thus obtainable can exceed those possible in discharge lasers by several orders of magnitude.

In the sections to follow, a theoretical analysis[9] of the vibrational relaxation and radiative gain in anharmonic oscillator expansions is first reviewed and provides a description of the physical details on which the operation of diatomic gasdynamic lasers depends. The analytical results also served as a guide to the choice of proper experimental conditions and allowed a selection of extreme gas mixtures to be made. The configuration and instrumentation of a shock-driven gasdynamic laser, similar to some CO_2 devices reported previously,[10,11] are described next, followed by the experimental performance with mixtures of CO. Finally, a brief discussion is included describing some unique features of diatomic gasdynamic lasers and their comparison to the characteristics of similar polyatomic (CO_2) systems.

VIBRATIONAL RELAXATION OF ANHARMONIC OSCILLATORS IN EXPANDING FLOWS

In their studies of the relaxation of anharmonically spaced vibrational quantum states, Treanor et al.[4] wrote the master equations for the population rate of each state. They included the usual terms accounting for collisional exchange of vibrational energy with the translational energy of the incident particle (V-T collisions), plus additional terms accounting for the exchange of vibrational energy between colliding oscillators (V-V collisions). They showed that in circumstances where the latter V-V terms dominate, the solution does not require Boltzmann population distributions but, to zeroth order, has the more general form

$$N_j^V = N_j^o \exp(\alpha V - E_j^V/kT) \qquad (1)$$

Here, N_j^V is the number density of oscillators of species j in vibrational quantum state V, E_j^V is the energy of that state above the ground state, T is the translational temperature, and α is an additional time-dependent

parameter. For the anharmonic Morse potential, the oscillator energy of quantum state V above the ground state is described by

$$E_j^V = k\theta_j V[1 - \varepsilon_j(V + 1)] \tag{2}$$

where θ_j is a characteristic vibrational constant of species j, and ε_j is a small anharmonic coefficient ($\varepsilon_j << \theta_j$). In vibrationally cooling nonequilibrium processes, α takes on growing positive values and, for small T, approaches the condition $\alpha \approx \theta_j/kT$. The product αV in equation (1) then nullifies the large linear terms in E_j^V and the resulting non-Boltzmann overpopulations of the upper states predicted by equation (1) are determined mainly by the magnitude of the small anharmonic coefficient, ε_j, in equation (2).

Recent "exact" numerical solutions to the complete master equations have been obtained for supersonic expansions of CO in mixture with other monatomic and diatomic gases.[9] The formulation of the rate equations for gas mixtures is similar to an approach reported by Bray[12] and are given with their related V-T and V-V transition probability expressions in appendix A. The numerical solutions reported here differ from those of Bray, however, who used a first-moment approximation to obtain solutions for a constant temperature process in N_2. These solutions contain no significant approximations and rely on a finite difference scheme for the numerical integration along an arbitrary one-dimensional flow axis.

An example of the results is shown in figure 1 for a CO expansion where the anharmonic CO population distribution at expansion area ratio $A/A_* = 200$ is compared with a harmonic oscillator solution and a distribution based on equation (1) for the same conditions. The anharmonic upper levels are significantly overpopulated when compared to the results of a harmonic oscillator model and, at larger area ratios, eventually become inverted. The distribution of the lowest levels is well described by the zeroth order approximation (eq. (1)) as predicted by Treanor et al.[4]

The addition of a second vibrationally relaxing species, with energy levels nearly resonant to those of CO, can enhance the upper level populations through additional V-V energy transfer. In particular, N_2 is suitable because it has slower V-T relaxation rates than CO, allowing N_2 to serve as a reserve of vibrational energy (in expansions) which may be efficiently (rapidly) transferred to the vibrational states of CO. Nitrogen therefore plays the same role with CO as with the asymmetric-stretch mode of CO_2 in all CO_2-N_2 lasers. The vibrational exchange between CO and N_2 does not depend on the anharmonicity of either species, however, although it can be strongly affected by anharmonicity. Teare et al.[13] derive an expression for the locally equilibrated V-V exchange between harmonic CO and N_2, in terms of vibrational temperatures, T_V:

$$T_{V_{CO}} = \frac{\theta_{CO}}{\frac{\theta_{N_2}}{T_{V_{N_2}}} - \frac{\theta_{N_2} - \theta_{CO}}{T}} \tag{3}$$

For sufficient vibrational excitation (large $T_{V_{N_2}}$) in the presence of low translational temperatures, the CO vibrational temperature or energy can become large and, in some cases, exceed its initial or reservoir value. An example of this vibrational pumping effect has been demonstrated experimentally[13] and is illustrated in figure 2 by some numerical examples for anharmonic CO and N_2. The influence of oscillator anharmonicity is to invalidate the accuracy of equation (3) for large area ratios. Figure 3 indicates the range of validity of equation (3) for these examples by comparing $(T_{V_{CO}})_{NUM}$, the numerically computed vibrational temperatures of anharmonic CO based on the relative population of the first and ground state levels, with $(T_{V_{CO}})_{Eq(3)}$, computed with equation (3) using local values of T and $T_{V_{N_2}}$ from the numerical solution. The net effect of N_2 on the population distributions of anharmonic CO is shown in figure 4, where a comparison is made with the previous 100-percent CO case. The 5-percent CO—95-percent N_2 mixture obtains a greater number of CO molecules in all levels above the fourth and displays a flatter distribution, both of which will contribute to greater radiative gain for transitions among those levels.

From the preceding, one may conclude that for expanding flows the effects of anharmonic energy states on the vibrational relaxation process must be included if populations of any (except the lowest) vibrational levels are of interest. Also, the addition of a second vibrationally resonant species can significantly enhance the overpopulation of upper vibrational states in the primary species. The latter effect leads to a similar enhancement of radiative gain, a feature discussed in detail in the next section.

INFRARED RADIATIVE GAIN IN DIATOMIC GAS EXPANSIONS

The formulation of radiative gain coefficients for Doppler broadened vibration-rotation transitions has been summarized by Patel[5] in connection with a CO electric discharge laser analysis. The molecular circumstances in gasdynamic lasers are slightly different, however, because they usually operate at higher pressures in the laser cavity. The combined effects of Doppler and collision broadening must then be considered. The formulation of radiative gain with both broadening mechanisms included is summarized in appendix B. The results are combined here with the previous vibrational relaxation calculations to provide an analysis of the radiative properties in diatomic gasdynamic expansions.

Following Patel,[5] some qualitative features of the P-branch vibration-rotation gain coefficients with only Doppler broadening are shown in figure 5 for a coefficient normalized by all of the multiplying molecular constants, which are independent of the upper level rotational quantum number, J, or rotational temperature, T_r. Note that the vibrational population ratio $X_j^V/X_j^{V-1} = 0.8$, used in figure 5, does not represent a net vibrational inversion; although as T_r decreases, positive gains appear and strengthen. In

the calculations to follow, gain coefficients are presented only for the P-branch rotational transition of maximum gain from each vibrational level.

Predicted gain coefficients are shown in figure 6 for several expanding CO-N_2 mixtures. As expected, expansions containing N_2 yield considerably higher gains than those with CO alone. Since optical loss coefficients for a moderate size research device are typically near 10^{-3} cm^{-1}, the results of figure 6 indicate that at the conditions assumed, CO expansions without N_2 can be made to lase only in unusually low-loss cavities and afford no advantages over those containing large fractions of N_2 where much greater gain is achieved.

A second aspect of the radiative properties from diatomic expansions is found in the gain enhancement due to reduced rotational temperatures as figure 5 indicates. Since rotational relaxation requires only a small number of collisions, the rotational energy (temperature) of most expansions may be assumed in thermal equilibrium with the local translational temperature. Thus, to enhance gain, the local translational temperature at a given geometric location in an expansion should be lowered without reducing the vibrational energy per molecule provided in the reservoir. This may be done through strictly thermodynamic effects by adding large fractions of a monatomic gas. Argon is particularly suitable for this purpose because, as a heavy collision partner, it also reduces the rate of vibrational energy loss to translation through V-T collisions. The enhancement of gain by diluting a 5-percent CO—95-percent N_2 mixture with 80-percent Ar is shown in figure 7. At area ratios less than 300, an order-of-magnitude increase in the gain coefficient is predicted and maximum gain occurs at transitions from lower vibrational levels.

The preceding results suggest three extreme gas mixtures to demonstrate the aspects of CO gasdynamic laser operation, namely, 100-percent CO, which is not expected to have sufficient gain except at very large area ratios ($A/A_* >> 200$); 25-percent CO—75-percent N_2, which yields ample gain and has the possible advantage of having the greatest system efficiency because the number of additional species not directly contributing energy to the laser states is minimized; and 80-percent Ar—5-percent CO—15-percent N_2, which should demonstrate the enhancement of gain over the previous mixture at lower area ratios and on radiative transitions from lower vibrational levels. These three gas mixtures were chosen for the experiments described in the following sections.

EXPERIMENTAL ARRANGEMENT

Mixtures of CO in N_2 and Ar were heated and supersonically expanded in the shock-tunnel arrangement illustrated in figure 8. The facility is operated by filling the driven tube with a test gas to pressures near 1 atm. A shock wave is generated in the tube by rupturing diaphragms separating it from a high-pressure (200 atm) helium driver. The incident wave reflects from the driven-tube end wall, leaving a stagnant volume of compressed and heated test gas that acts as the nozzle reservoir and remains nearly undisturbed for

several milliseconds. The compressed reservoir gas ruptures a thin copper diaphragm and exhausts into the evacuated nozzle and dump tank. Expansion waves and helium from the driver then arrive and destroy the steady reservoir conditions. The nozzle was an axisymmetric 10° (half-angle) cone with a 1.27 cm^2 sonic throat area, A_*. Mirror ports, with their optical axis perpendicular to the flow axis, were located at geometrical area ratios, A/A_*, of 577, 1455, and 2730. An optical cavity could be provided in any one of the ports by installing two circular mirrors, each with a 4.4-cm-diameter aperture and an inside spherical surface of 10-m radius. Power was removed through one mirror, made from a germanium substrate and coated for 3-percent transmission over the spectral region between 5 and 6 μm. Transmissivity rose through 14 percent at 4.7 μm. The other mirror was coated for maximum reflectivity over the same spectral region.

Laser power was determined during the 2 ms period of quasi-steady flow by monitoring the temporal profile of the intensity pulse and measuring its total energy.[11] The intensity pulse was monitored with a fast-response Ge:Au detector viewing an attenuated fraction of the beam reflected from a CaF_2 beam splitter. The transmitted laser power (93 percent) was absorbed by a calibrated copper slug calorimeter. The combined pulse shape and energy measurements provided absolute time-dependent power values with an experimental accuracy of at least ±20 percent at 100 W. The minimum power that could be resolved was less than 5 W.

Spectral measurements were made with a wide-band, grating monochrometer set at a different central wavelength for each run. The collimated laser beam illuminated a NaCl diffusing plate located ahead of the entrance slit to help fill the instrument optics. A 75-groove/mm grating, blazed at 8 μm, was used in second order with a 1-mm exit slit, giving a measured band pass of 0.08 μm. The 5-μm shock-tunnel spectral signals were detected by a Ge:Au detector with a 1-mm-square cold aperture and a uniform spectral response between 4.5 and 6 μm. The monochrometer band-pass measurements could not be made using the Ge:Au detector, however, and the shock-tunnel data showed evidence that a smaller band pass existed, apparently limited by the external detector optics. Hence, all spectral features may not appear in the experimental results although the major features not found initially were located by additional intermediate wavelength settings.

Since hydrogen-bearing impurities are believed to have a large effect on vibrational relaxation rates, particularly in CO expansions,[14] attention was given to the test gas purity. Matheson "ultra-high" purity CO and Ar and "prepurified" N_2 were mixed, as received, in an evacuated and outgassed mixing tank several days prior to their use. The driven tube was also purged with N_2 and evacuated before loading. These procedures are not sufficient to achieve the slowest vibrational relaxation rates reported by von Rosenberg et al.,[14] but represent a practical limit for convenient gasdynamic laser operation. From von Rosenberg's data,[14] the conditions of these experiments are assumed to yield CO vibrational relaxation rates up to 100 times faster than the slowest possible and consequently have an adverse effect on radiative gain.

EXPERIMENTAL RESULTS

Of the gas mixtures used (100-percent CO, 25-percent CO—75-percent N_2, and 5-percent CO—15-percent N_2—80-percent Ar), only those containing N_2 resulted in laser operation. Examples of the instrumentation response to runs with the successful mixtures are shown in figure 9. The reservoir radiation (upper traces) was monitored with an InSb detector, through a 2-μm, wide-band, filter and quartz window located in the driven-tube side wall near the nozzle entrance. The reservoir radiation traces provide an indication of the combined variations of reservoir temperature and pressure. The reservoir pressures (middle traces) were measured with a calibrated piezoelectric transducer in a similar location. They indicate the arrival of the incident shock wave (small step), followed by a large pressure step behind the reflected wave. Nearly-constant reservoir pressures were obtained for 2 to 3 ms in most cases, even for the off-tailored conditions of figure 9(b). The nozzle required about 0.5 ms to start as the delayed laser intensity in the lower traces indicate. Laser radiation originated from the starting shock wave and varied afterward in accordance with the reservoir conditions. The beam apparently contained a multitude of transverse modes since the beam size was between 1.5 and 2.0 cm, 10 times the predicted single-mode size. Experiments with only the output mirror installed gave no signal in the Ge:Au monitor, verifying that the detected radiation came only from intense laser transitions. Note that while the laser radiation from the 80-percent Ar mixture (fig. 9(b)) decays soon after arrival of disturbances in the reservoir, the mixture with only CO and N_2 (fig. 9(a)) continues to lase until most of the reservoir is exhausted. The extended period of the latter mixture is partly explained by a comparison of the spectral intensities in figure 10.

The spectral intensities at all wavelengths from the 80-percent Ar mixtures were found to decay within 11 ms after starting (fig. 10(a)). The 25-percent CO—75-percent N_2 mixture, however, exhibited a first peak concurrent with the multimode intensity, followed by a second more intense peak for some wavelengths. The second peak consistently occurred 11 ms after starting. The double spectral behavior of the 25-percent CO—75-percent N_2 mixture is believed to be caused by the mixing of driver He with the test gas. Since He is a monatomic gas, it also enhances the gain, although it increases the rate of vibrational energy transfer to translation. The adverse effects of He could not have been too great, however, since the total multimode intensity at 11 ms is reduced mainly in accordance with the reduced reservoir pressure. The spectral characteristics of all the mixtures at $A/A_* = 2730$, including those with the unknown He content, are summarized in figure 11. The CO-N_2-He data represent the peak intensities 11 ms after starting, while the others were measured at 2 ms. In all cases, the intensities at each wavelength have been normalized by the maximum obtained at 2 ms and by the small variations in total multimode intensity from run to run. The spectral regions of each vibrational transition are also indicated in figure 11 for the P(4) to P(12) rotational lines. At $A/A_* = 2730$, the 25-percent CO—75-percent N_2 mixture lases most intensely near 5.05 μm, suggesting the transition of maximum gain to be from the sixth vibrational level. After 11 ms, the 5.05-μm radiation is completely quenched and the shorter wavelengths are enhanced, in accordance with the effects of a monatomic additive (viz., He). The most intense radiation

from the 80-percent Ar mixture was near 4.78 μm, suggesting the transition of maximum gain to be from the second vibrational level. Laser operation at lower wavelengths was suppressed, however, by the increased reflection losses of the mirror coatings below 5 μm (14 percent at 4.7 μm) and possibly by strong boundary-layer absorption of the 1,0 vibrational transitions. The spectral data in figure 11 are corroborated by the gain predictions in figure 12. Those calculations were done for the conditions of the experiment but used V-T rates 100 times faster than the established postshock wave values for both CO and N_2. The calculations may therefore underpredict gain but are more compatible with the vibrational relaxation data for CO expansions reported by Russo[15] and von Rosenberg et al.[14] A comparison of figures 11 and 12 shows the spectral behavior of the laser to be consistent with the predicted transitions of maximum gain and gain distribution over the vibrational states. In all cases, the predicted gain corresponds to only partial inversions of the vibrational states and increases with area ratio.

The total multimode laser power (from all wavelengths combined) varied with the expansion area ratio as figure 13 shows. The data reflect the predicted increase in gain with area ratio but are distorted by the effect of a decreasing fraction of flow passing between the laser mirrors as area ratio increases; that is, at the larger area ratios, most of the flow passes above and below the internal beam where its latent power cannot be extracted. The data may be compared with the projected performance of other nozzle configurations (e.g., two-dimensional nozzles where most of the flow passes through the internal beam) and with the measured performance of some similar CO_2 gasdynamic lasers[11,16] by recasting it in terms of an efficiency based on the total enthalpy flow rate through the internal beam. This efficiency would then equal the ratio of laser power obtainable in a properly designed nozzle to the total power required to heat the nozzle reservoir gases. For these experiments, efficiency is defined by

$$\text{Eff} = \frac{P}{H_o \dot{m}} \frac{A}{LD} \tag{4}$$

where P is the measured laser power, H_o is the reservoir specific enthalpy, $\dot{m}$ is the mass-flow rate through the nozzle, A is the nozzle cross section containing the optical axis, and L and D are the length and average diameter of the internal laser beam intersected by the flow. Efficiency percentages, computed from the power data in figure 13, are compared in figure 14 with the optimum output of two CO_2 gasdynamic lasers operated at Ames Research Center.* On this basis, the nonoptimized CO gasdynamic laser reported here is seen to match or exceed the capabilities of similar CO_2 devices. All of the lasers represented in figure 14 operated at reservoir enthalpy flow rates, $H_o\dot{m}$, between 1 and 3 MW.

The influence of varying reservoir conditions is shown in figures 15 and 16. The maximum reservoir pressure (170 atm) was limited by the apparatus and no upper power level was achieved. The optimum reservoir temperature, for the 80-percent Ar mixture (computed from incident shock speed measurements), appears to be near 2000° K.

---

*Unpublished data taken from an arc-heated CO_2 gasdynamic laser by G. Lee.

A second output mirror, coated for 10-percent transmission between 5 and 6 μm, also supported laser operation at $A/A_* = 1455$ and gave approximately the same output power. The ideal mirror transmission will depend on the nozzle configuration, area ratio, and desired spectral characteristics, however, and was not investigated further.

SUMMARY AND APPLICATION CONSIDERATIONS

The preceding experiments have provided evidence that supports the qualitative nature of predictions based on recent anharmonic oscillator vibrational relaxation theories. Laser radiation, which depends on partial vibrational inversions induced in the thermal expansion of anharmonic CO, has been measured at wavelengths corresponding to a multitude of lower vibrational transitions. Multimode power levels were obtained that match or exceed the performance of similar CO_2 gasdynamic lasers.

Some unique features are provided by diatomic gasdynamic lasers operating on the vibrational energy states of a single vibrational mode. For example, laser transitions occurring between the upper vibrational levels, V and V-1, cause an enhanced inversion between the V-1 and V-2 levels. Likewise, the relative populations between V+1 and V are also further inverted. Thus, the removal of laser power from one location in a CO expansion should enhance the gain at several different wavelengths farther downstream. This behavior is in contrast to the performance of a CO_2 system operating on the lowest excited levels of two vibrational modes. There, the maximum efficiency or laser power must be obtained by using cavity mirrors extended in the flow direction. The laser power is then controlled by the collisional transfer rate of vibrational energy from N_2 to the CO_2 asymmetric-stretch mode (the upper laser level). The CO gasdynamic laser may therefore have the advantage of either providing equal amounts of laser power from laser cavities with shorter lengths in the flow direction or allow single-mode laser power for a multitude of wavelengths, with each wavelength from a cavity at a different location in a single expansion. These features accompany the disadvantages associated with the increased atmosphere absorption at 5 μm compared to that at 10.6 μm and the required disposition of large amounts of toxic CO from the nozzle exhaust.

Ames Research Center
National Aeronautics and Space Administration
Moffett Field, Calif., 94035, Oct. 1, 1970

APPENDIX A

MASTER RATE EQUATIONS

RATE EQUATIONS

The number density of oscillators, N_j^V, of species j in vibrational quantum state V may be expressed in terms of a mole fraction, X_j^V, relative to the entire gas mixture, that is,

$$X_j^V = \frac{N_j^V}{\sum_{j,v} N_j^V} \tag{A1}$$

In general terms, the temporal rate of change of X_j^V due to a collisional relaxation process may be written

$$\frac{dX_j^V}{dt} = \sum_k Z_{jk} Q_{jk}^V \tag{A2}$$

where Q_{jk}^V is the molar production per collision of X_j^V due to encounters between species j and k, and Z_{jk} is an average collision rate given by

$$Z_{jk} = \frac{\rho}{m} d_{jk}^2 \sqrt{\frac{8\pi kT}{\mu_{jk}}} \tag{A3}$$

In equation (A3), ρ and m are the average fluid density and molecular weight, d_{jk}^2 is a collision cross section for encounters between species j and k, and μ_{jk} is their reduced mass. If we denote the total mole fraction of species k as $\hat{X}_k = \sum_L X_k^L$, including all vibrational quantum states L, and consider only single quantum transitions, the production term due to vibration-to-translation (V-T) energy exchanges becomes

$$\left[Q_{jk}^V\right]_{V-T} = \hat{X}_k P_{jk}^{1,0} \left\{ \bar{P}_{jk}^{V,V-1} \left[X_j^{V-1} \exp\left(-E_j^{V,V-1}/kT\right) - X_j^V \right] + \bar{P}_{jk}^{V+1,V} \left[X_j^{V+1} - X_j^V \exp\left(-E_j^{V+1,V}/kT\right) \right] \right\} \tag{A4a}$$

The vibration-to-vibration (V-V) energy transfer contributes

$$\left[Q_{jk}^{V}\right]_{V-V} = P_{jk}\binom{0,1}{1,0} \sum_{L} \left\{ \overline{P}_{jk}\binom{L,L+1}{V,V-1} \left[X_j^{V-1} X_k^{L+1} \exp\left(E_k^{L+1,L}/kT - E_j^{V,V-1}/kT\right) - X_j^{V} X_k^{L} \right] \right.$$

$$\left. + \overline{P}_{jk}\binom{L,L+1}{V+1,V} \left[X_j^{V+1} X_k^{L} - X_j^{V} X_k^{L+1} \exp\left(E_k^{L+1,L}/kT - E_j^{V+1,V}/kT\right) \right] \right\} \tag{A4b}$$

and the total production term is then

$$Q_{jk}^{V} = \left[Q_{jk}^{V}\right]_{V-T} + \left[Q_{jk}^{V}\right]_{V-V} \tag{A4c}$$

Equations (A4) include the detailed balance relations, exemplified by

$$P_{jk}^{V-1,V} = P_{jk}^{V,V-1} \exp\left(-E_j^{V,V-1}/kT\right)$$

and are written in terms of relative transition probabilities

$$\left.\begin{aligned} \overline{P}_{jk}^{r,s} &= P_{jk}^{r,s}/P_{jk}^{1,0} \\ \overline{P}_{jk}\binom{\ell,m}{r,s} &= P_{jk}\binom{\ell,m}{r,s}/P_{jk}\binom{0,1}{1,0} \end{aligned}\right\} \tag{A5}$$

for later convenience.

Terms similar to $E_j^{V,V-1}$ in equations (A4) are the energy difference between two adjacent states, V and V-1, of species j. They may be evaluated by assuming a Morse oscillator model in which the vibrational energy above the ground state is given by

$$E_j^{V} = k\theta_j V[1 - \varepsilon_j(V + 1)] \tag{A6a}$$

Here, θ_j is a characteristic vibrational temperature and ε_j is the small anharmonic coefficient. The energy difference, $E_j^{V,V-1}$ is then

$$E_j^{V,V-1} = k\theta_j(1 - 2\varepsilon_j V) \tag{A6b}$$

TRANSITION PROBABILITIES

Following Bray,[12] we can adopt a convenient form of the theory of Schwartz et al.,[16] in which the probability ratios are given by

$$\bar{P}_{jk}^{V,V-1} = V\left(\frac{1 - \epsilon_j}{1 - V\epsilon_j}\right)\frac{F_j^V}{F_j^1} \tag{A7a}$$

$$\bar{P}_{jk}\binom{L,L+1}{V,V-1} = V(L+1)\left(\frac{1 - \epsilon_j}{1 - V\epsilon_j}\right)\left(\frac{1 - \epsilon_k}{1 - L\epsilon_k}\right)\frac{F_{jk}^{V,L}}{F_{jk}^{1,0}} \tag{A7b}$$

The integral expressions of the adiabaticity factors F_j^V and $F_{jk}^{V,L}$ are evaluated by an empirical fit of Keck and Carrier[17] which bridges the gap between impulsive and adiabatic energy exchange, namely,

$$F = \frac{1}{2}\,(3 - e^{-2/3\lambda})e^{-2/3\lambda} \tag{A8}$$

In equation (A8), λ is given by

$$\lambda_{jk} = \frac{2\pi^2 \ell_j}{h}\,|\Delta E_{jk}|\sqrt{\frac{\mu_{jk}}{2kT}} \tag{A9}$$

where ℓ_j is a range parameter describing the intramolecular potential and $|\Delta E_{jk}|$ is the magnitude of the net vibrational energy difference for the exchange in question. Equations (A4) also require absolute values of the ground state probabilities, $P_{jk}^{1,0}$ and $P_{jk}\binom{0,1}{1,0}$. Since, in many cases, existing theories do not successfully reproduce the experimental results, preference is given here to the experimental values in an empirical form. Data are available, at least for the $P_{jk}^{1,0}$ values, obtained from measurements of the net relaxation time, τ_{jk}, behind the shock waves. Under the conditions of shock-wave experiments, τ_{jk} depends principally on $P_{jk}^{1,0}$ alone, allowing the latter to be determined with the correlation

$$\tau_{jk} = \frac{B_{jk}}{p}\exp(C_{jk}T^{-1/3}) \tag{A10}$$

and

$$P_{jk}^{1,0} = \left[\tau_{jk}p\; d_{jk}^2 \hat{X}_k \sqrt{\frac{8\pi}{\mu_{jk}kT}}\,(1 - e^{-\theta_j/T})\right]^{-1} \tag{A11}$$

Values of the empirical constants, B_{jk} and C_{jk}, used in this study were determined from the data of Millikan, White, and Hooker.[18,19]

Experimental data for the V-V probability $P_{jk}\left(\begin{smallmatrix}0,1\\1,0\end{smallmatrix}\right)$ are more sparse. However, what little is pertinent to this work (e.g., refs. 20 and 21) shows that convenient closed-form expressions like those of Schwartz et al.[16] are usually suitable for predicting the temperature dependence of $P_{jk}\left(\begin{smallmatrix}0,1\\1,0\end{smallmatrix}\right)$ but must often be adjusted in magnitude. We shall adopt that point of view here and obtain expressions for $P_{jk}\left(\begin{smallmatrix}0,1\\1,0\end{smallmatrix}\right)$ from the following: Schwartz et al.[16] describe the transition probabilities for V-V transfer between energy levels - far from resonance - as

$$P_{jk}\left(\begin{smallmatrix}0,1\\1,0\end{smallmatrix}\right) = 0.39\pi^2 \frac{\mu_{jk}^2}{M_j M_k} \frac{(\Delta E_{jk})^2}{E_j^1 E_k^1} \frac{\sigma_{jk}^{3/2}\, e^{-\sigma_{jk}}}{1 - e^{-2/3\sigma_{jk}}} \tag{A12a}$$

where

$$\sigma_{jk} = 3\left[\frac{2\pi^4 \mu_{jk} \ell_{jk} (\Delta E_{jk})^2}{h^2 kT}\right]^{1/3} - \frac{\Delta E_{jk}}{2kT} \tag{A12b}$$

and

$$\Delta E_{jk} = \left| E_j^1 - E_k^1 \right|$$

In equations (A12), M_j is the reduced mass of the oscillator j, and E_j^1 is its energy given by equation (A6) for $V = 1$. For the near-resonant case, Treanor[22] reports a modified version of the theory in reference 16 for small energy differences which reduces to the theory of reference 16 for exact resonance, namely,

$$P_{jk}\left(\begin{smallmatrix}0,1\\1,0\end{smallmatrix}\right) = \frac{\mu_{jk} h^2 kT\, e^{-\Omega_{jk}}}{4\pi^2 M_j M_k \ell_j \ell_k E_j^1 E_k^1} \tag{A13a}$$

where

$$\Omega_{jk} = \frac{8\pi^4}{25} \ell_{jk}^2 \mu_{jk} \frac{(\Delta E_{jk})^2}{h^2 kT} \tag{A13b}$$

As Treanor[22] points out, when either equations (A12) or (A13) are used away from the region in which they apply, the prediction is too small. Later comparisons to the data of reference 21 showed values of 1/10 the larger of the results given by equations (B12) and (B13) to provide a reasonable estimate. Those were the values used here. The appropriate molecular constants are listed in table 1.

TABLE 1.- TRANSITION PROBABILITY CONSTANTS

Species	θ_j (°K)	ε_j	d_j^2 (cm^2)	ℓ_j (cm)
CO	3122	6.203×10^{-3}	1.36×10^{-15}	2.00×10^{-9}
N_2	3395	6.217×10^{-3}	1.38×10^{-15}	2.03×10^{-9}
Ar	-	-	6.75×10^{-16}	2.00×10^{-9}

APPENDIX B

RADIATIVE GAIN COEFFICIENTS FOR THE VIBRATION-ROTATION BANDS OF DIATOMIC MOLECULES

Radiative properties for laser applications are conveniently described in terms of a small-signal spectral gain coefficient defined by

$$k(\nu) = \frac{d}{dz} (\ell n\ I_\nu) \tag{B1}$$

where z is the optical path coordinate and I_ν is the spectral intensity at frequency, ν. Since laser oscillation preferentially seeks the frequency of maximum gain (the line center) and gain measurements are most often made with the spontaneous emission nulled, the expression for gain coefficient in this application refers only to induced transitions at the line-center frequency, ν_o. In terms of the local molecular properties, we can then write

$$k(\nu_o) = N_u h\nu_o B_{u\ell} \eta_{u\ell}(\nu_o) \left[1 - \frac{g_u N_\ell}{g_\ell N_u}\right] \tag{B2}$$

where N_u and N_ℓ are the number densities for the upper and lower radiative states, g_u and g_ℓ are their degeneracies, $B_{u\ell}$ is an Einstein coefficient for induced emission, and $\eta_{u\ell}(\nu_o)$ is the corresponding normalized line-shape function, evaluated at the line-center frequency, ν_o. For purely Doppler broadened lines, usually considered in most laser applications, Penner[23] shows that

$$\eta_{u\ell}(\nu_o) = \frac{2}{\Delta\nu_D} \sqrt{\frac{\ell n\ 2}{\pi}} \tag{B3}$$

where the Doppler line width is

$$\Delta\nu_D = \frac{2\nu_o}{c} \sqrt{2\ \ell n\ 2\ \frac{kT}{m}} \tag{B4}$$

At most of the gasdynamic laser conditions, collisional broadening also becomes significant. The combined collision and Doppler broadened line profiles, evaluated at the line center, are shown by Penner[23] to be

$$\eta_{u\ell}(\nu_o) = \frac{2}{\Delta\nu_D} \sqrt{\frac{\ell n\ 2}{\pi}}\ e^{x^2}[1 - \mathrm{erf}(x)] \tag{B5}$$

where $x = \sqrt{\ell n\ 2}(\Delta\nu_c/\Delta\nu_D)$ and the collision line width for species j is

$$\Delta\nu_c = \frac{1}{\pi} \frac{\rho}{m} \sum_k \hat{X}_k \delta_{jk} \left(\frac{8\pi kT}{\mu_{jk}}\right)^{1/2} \tag{B6}$$

Values of the optical cross section, δ_{jk}, are listed in table 2 and reference 23 for the gases of interest here.

Equations (B2) through (B6) may be specialized to the vibration-rotation spectra of a three-dimensional rigid rotor, anharmonic oscillator for vibration-rotation transitions; $u \rightarrow \ell = (V,J) \rightarrow (V-1,J\pm1)$ where V and J are the principal vibration and rotation quantum numbers. In this case, the Einstein coefficients, $B_{u\ell}$, for degenerate rotation-vibration states with the selection rule, $\Delta J = \pm 1$, are correlated by

$$B_{u\ell} = B_{10}V\left(\frac{J + n}{2J + 1}\right) \tag{B7}$$

where

$$n = \begin{cases} 0, \ \Delta J = -1 \ \text{(R-branch)} \\ 1, \ \Delta J = +1 \ \text{(P-branch)} \end{cases}$$

Since the P-branch gain coefficients are always greater, only $\Delta J = +1$ transitions will be considered further. The molecular constant, B_{10}, is determined from values of the commonly measured Einstein coefficients for spontaneous emission, $A_{u\ell}$, at wavelength $\nu_{u\ell}$, through the relation

$$B_{10} = \frac{c^2}{2h\nu_{u\ell}^3} \frac{A_{u\ell}}{V\left(\frac{J + n}{2J + 1}\right)} \tag{B8}$$

The ratio $g_u N_\ell / g_\ell N_u$ in equation (B2) is evaluated by assuming that the rotational states are populated according to a locally equilibrated Boltzmann distribution. On that basis, we denote the mole fraction of molecules in the combined rotation-vibration state, V and J, as $X^{V,J}$ and define $X^V = \sum_j X^{V,J}$, which is identical to the vibrational mole fraction, X_j^V, previously computed. If $\Delta E^{V,J}$ is the difference in energy between the Jth rotational state of level V and the ground rotational state of level V, then

$$\frac{X^{V,J}}{g_J} = \frac{X^V \exp(-\Delta E^{V,J}/kT)}{Q_r(T)} \tag{B9}$$

where $Q_r(T)$ is a rotational partition function given by $Q_r = T/\theta_r$ and the energy difference is

$$\Delta E^{V,J} = k\theta_r J(J + 1)\left[1 - \delta_r\left(V + \frac{1}{2}\right)\right] \tag{B10}$$

In the above, θ_r is a characteristic rotational temperature defined in Herzberg's spectroscopic notation[24] as $\theta_r = hcB_e/k$ and $\delta_r = \alpha_e/B_e$. The ratio, $g_u N_\ell / g_\ell N_u$, for fundamental P-branch transitions is then equal to

$$\frac{g_J X^{V-1,J+1}}{g_{J+1} X^{V,J}} = \frac{X^{V-1}}{X^V} \exp\left[\left(\Delta E^{V,J} - \Delta E^{V-1,J+1}\right)/kT\right] \tag{B11}$$

Similarly, the upper level number density in equation (B2) may be written

$$N_u = \frac{\rho}{m} (2J + 1) \frac{X^V \exp(-\Delta E^{V,J}/kT)}{T/\theta_r} \tag{B12}$$

The formulation given by equations (B2) to (B12) is sufficient to compute $k(\nu_o)$ for $\Delta V = 1$, P-branch transitions, in terms of ρ, T, and X^V_j. The necessary radiation constants are listed in table 2 for CO.

TABLE 2.- CO RADIATIVE CONSTANTS

B_{10} (cm^2/erg sec)	θ_r (°K)	δ_r	δ_{jk} (cm^2):k=CO	k = N_2	k = Ar
*6.02×10^5	2.778	9.05×10^{-3}	5.3×10^{-15}	5.3×10^{-15}	1.7×10^{-15}

*Based on $A(v, j:v-1, j-1) = 1.14$ sec^{-1} for $v = 1$; $j = 7$ at $\nu_o = 2169$ cm^{-1} (ref. 24).

REFERENCES

1. Landau, L.; and Teller, E.: Theory of Sound Dispersion. Phys. zeits. d. Sowjetunion, 10.1, 1936, pp. 34-43.

2. Basov, N. G.; Mikhaylov, V. G.; Orayevsky, A. N.; and Shcheglov, V. A.: Molecular Population Inversion in the Supersonic Flow of a Binary Gas in a Level Nozzle. Translation Source Zhurnal Tecknicheskoy Fiziki, vol. 38, no. 12, 1968, pp. 2031-2041; Soviet Phys.-Tech. Phys., vol. 13, 1969, pp. 1630-1636.

3. Anderson, J. D., Jr.: A Time-Dependent Quasi-One-Dimensional Analysis of Population Inversions in an Expanding Gas. U. S. Naval Ordnance Lab. Rep. NOLTR 69-200, Dec. 1969.

4. Treanor, C. E.; Rich, J. W.; and Rehm, R. G.: Vibrational Relaxation of Anharmonic Oscillators with Exchange-Dominated Collisions. J. Chem. Phys., vol. 48, no. 4, Feb. 15, 1968, pp. 1798-1807.

5. Patel, C. K. N.: Vibrational-Rotational Laser Action in Carbon Monoxide. Phys. Rev., vol. 141, no. 1, Jan. 1966, pp. 71-83.

6. Legay, Francois: Study of a CO-N_2 Laser by a Method of Modulation. C. R. Acad. Sci., Paris, Serie B, t. 266, Feb. 26, 1968, p. 554.

7. Osgood, R. M., Jr.; Eppers, W. C., Jr.; and Nichols, E. R.: An Investigation of the High Power CO Laser. VOLQE-6, no. 3, March 1970, pp. 145-154.

8. Jeffers, W. Q.; and Wiswall, C. E.: A Transverse-Flow CO Chemical Laser. Appl. Phys. Let., vol. 17, no. 2, July 15, 1970, pp. 67-69.

9. McKenzie, R. L.: Vibrational Relaxation and Radiative Gain in Expanding Flows of Anharmonic Oscillators. NASA TN D- , 197 .

10. Anon.: Physics Today, July 1970, p. 55.

11. Kuehn, D. M.; and Monson, D. J.: Experiments with a CO_2 Gasdynamic Laser. Appl. Phys. Let., vol. 16, no. 48, 1970.

12. Bray, K. N. C.: Vibrational Relaxation of Anharmonic Oscillator Molecules: Relaxation Under Isothermal Conditions. J. Phys. B. (Proc. Phys. Soc.), Ser. 2, vol. 1, 1968, pp. 705-717.

13. Teare, J. D.; Taylor, R. L.; and von Rosenberg, C. W., Jr.: Observations of Vibration-Vibration Energy Pumping Between Diatomic Molecules. AVCO Everett Res. Lab. Rep. AMP 268, Oct. 1969.

14. Von Rosenberg, C. W.; Taylor, R. L.; and Teare, J. D.: Vibrational Relaxation of CO in Nonequilibrium Nozzle Flow. J. Chem. Phys., vol. 48, 1968, pp. 5731-5733.

15. Russo, Anthony L.: Spectrophotometric Measurements of the Vibrational Relaxation of CO in Shock-Wave and Nozzle Expansion-Flow Environments. J. Chem. Phys., vol. 47, no. 12, Dec. 15, 1967, p. 5201.

16. Schwartz, R. N.; Slawsky, Z. I.; and Herzfeld, K. F.: Calculation of Vibrational Relaxation Times in Gases. J. Chem. Phys., vol. 20, no. 10, Oct. 1952, pp. 1591-1599.

17. Keck, J.; and Carrier, G.: Diffusion Theory of Nonequilibrium Dissociation and Recombination. J. Chem. Phys., vol. 43, no. 7, Oct. 1, 1965, pp. 2284-2288.

18. Millikan, R. C.; and White, D. R.: Systematics of Vibrational Relaxation. J. Chem. Phys., vol. 39, no. 12, Dec. 15, 1963, pp. 3209-3213.

19. Hooker, W. J.; and Millikan, R. C.: Shock-Tube Study of Vibrational Relaxation in Carbon Monoxide for the Fundamental and First Overtone. J. Chem. Phys., vol. 38, no. 1, Jan. 1, 1963, pp. 214-220.

20. Taylor, R. L.; and Bitterman, S.: Survey of Vibrational Relaxation Data for Processes Important in the CO_2-N_2 Laser System. AVCO Everett Res. Lab. Rep. 282, Oct. 1967.

21. Taylor, R. L.; Camac, M.; and Feinberg, R. M.: Measurements of Vibration-Vibration Coupling in Gas Mixtures. Proc. of Eleventh Symposium on Combustion (International), Aug. 15-19, 1966, Berkeley, California.

22. Treanor, C. E.: Coupling of Vibration and Dissociation in Gasdynamic Flows. AIAA Paper 65-29, 1965.

23. Penner, S. S.: Quantitative Molecular Spectroscopy and Gas Emissivities. Addison-Wesley Pub. Co., Inc., 1959.

24. Herzberg, G.: Molecular Spectra and Molecular Structure, I. Spectra of Diatomic Molecules. D. Van Nostrand Co., Inc., 1950.

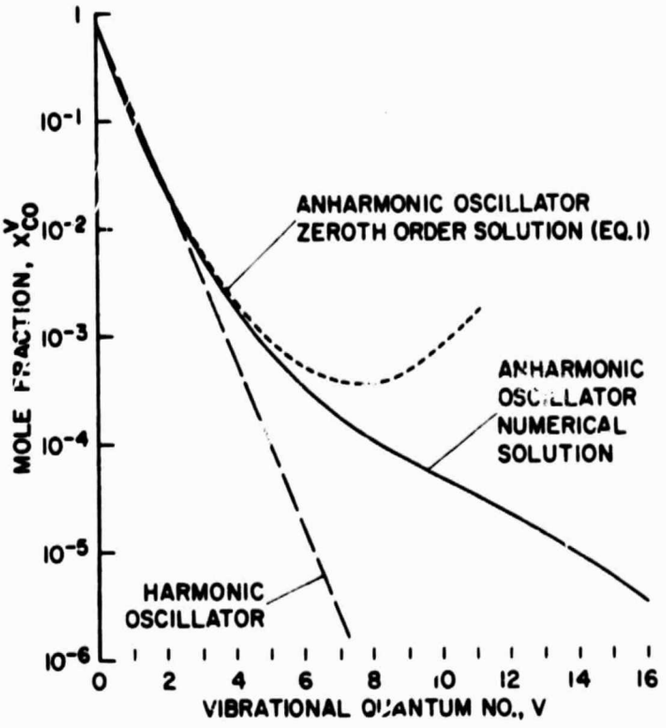

Figure 1.- Population distributions at $A/A_* = 200$ for harmonic and anharmonic CO expanding in a two-dimensional supersonic nozzle with a 15° divergence half-angle and a 0.127-cm throat height. Reservoir conditions were $P_o = 100$ atm and $T_o = 2000°$ K.

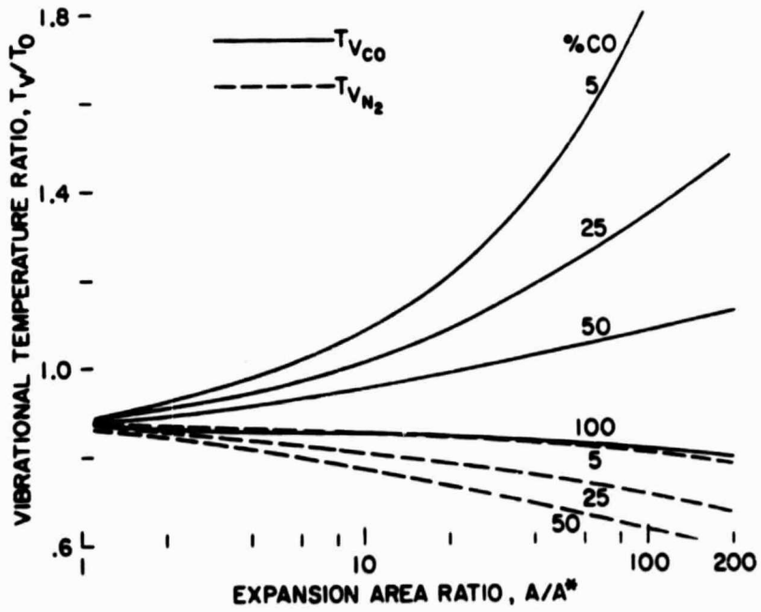

Figure 2.- Vibrational temperatures normalized by the reservoir temperature, T_o, in expansions of anharmonic CO-N_2 mixtures. The vibrational temperatures are determined from the relative populations of the first and ground vibrational energy state of each species. (Nozzle conditions are the same as for fig. 1.)

NATIONAL AERONAUTICS AND SPACE ADMINISTRATION
AMES RESEARCH CENTER, MOFFETT FIELD, CALIFORNIA

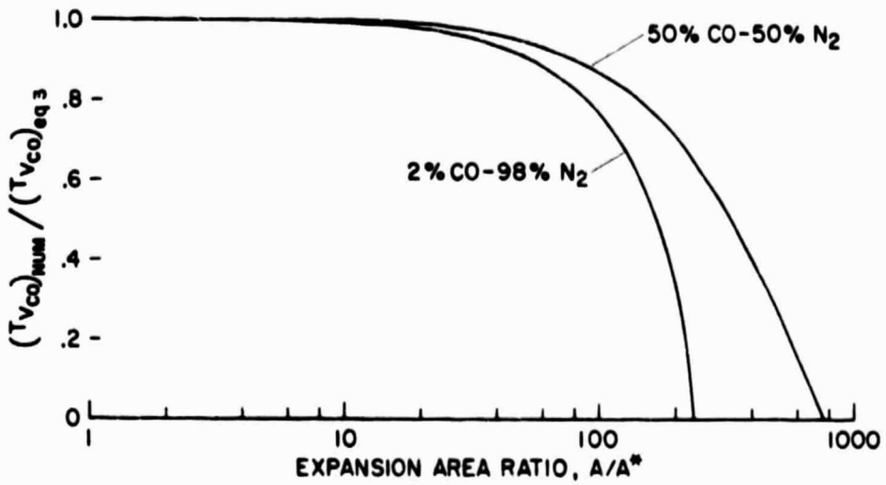

Figure 3.- Comparison of the CO vibrational temperature for a harmonic oscillator model calculated from equation (3) and the anharmonic CO vibrational temperature of the first and ground state populations from numerical solutions. (Nozzle conditions are the same as fig. 1.)

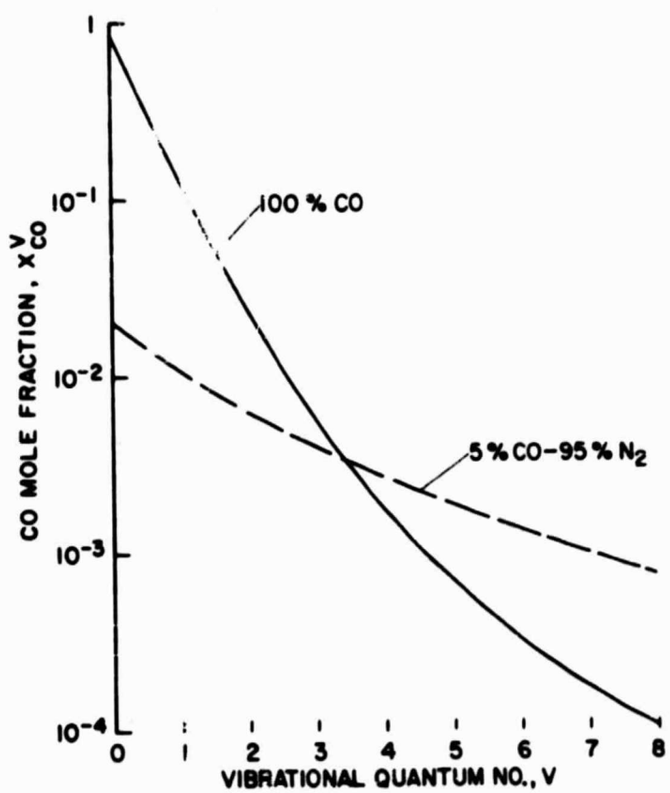

Figure 4.- The effect of N_2 on the population distributions of CO at $A/A_* = 200$. (Nozzle conditions are the same as for fig. 1.)

NATIONAL AERONAUTICS AND SPACE ADMINISTRATION
AMES RESEARCH CENTER, MOFFETT FIELD, CALIFORNIA

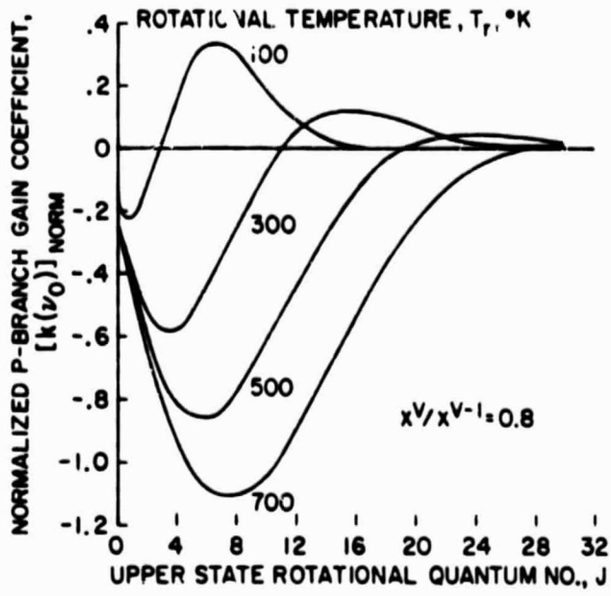

Figure 5.- Normalized P-branch gain coefficients for Doppler-broadened vibration-rotation transitions from a partial ($x^V/x^{V-1} < 1$) vibrational inversion.

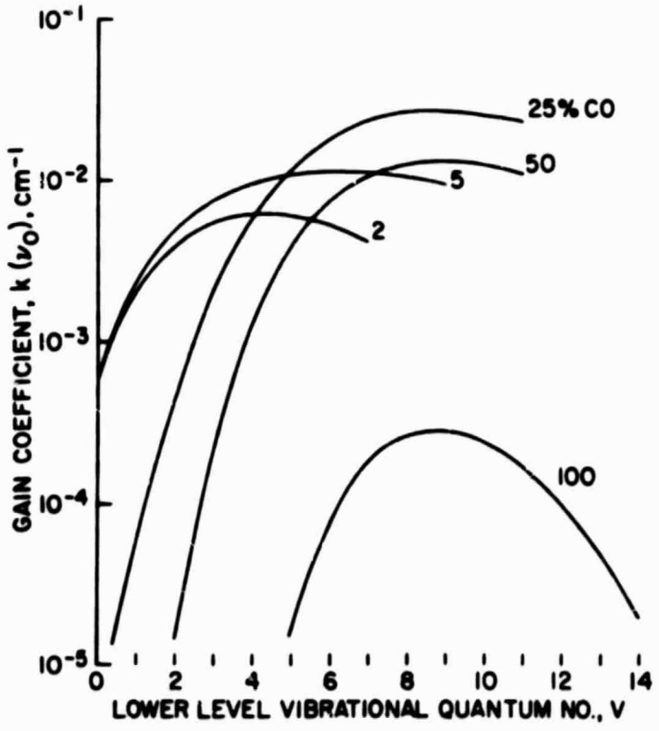

Figure 6.- CO gain coefficients at $A/A_* = 200$ in CO-N_2 expansions. (Nozzle conditions are the same as for fig. 1.)

NATIONAL AERONAUTICS AND SPACE ADMINISTRATION
AMES RESEARCH CENTER, MOFFETT FIELD, CALIFORNIA

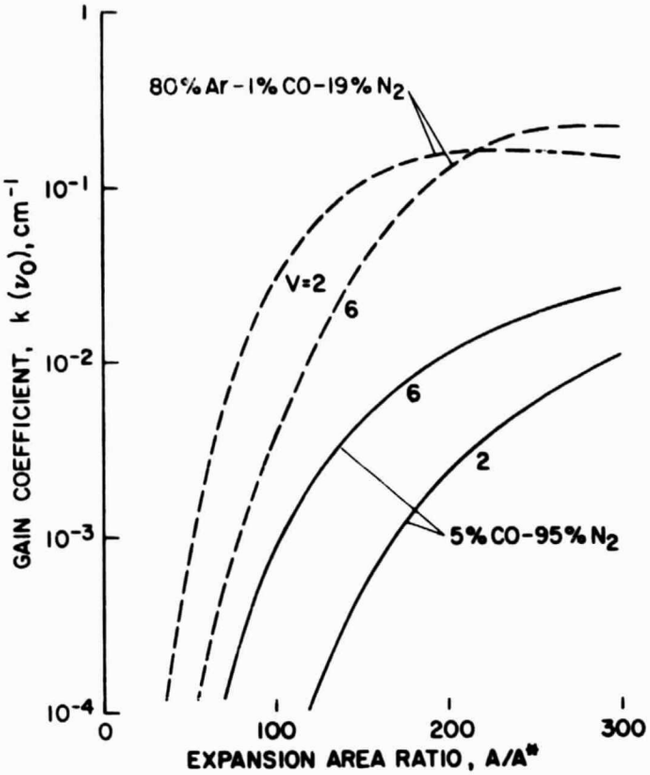

Figure 7.- The effect of Ar dilution on CO gain coefficients in CO-N_2-Ar expansions. V is the upper level vibrational quantum number. (Nozzle conditions are the same as in fig. 1.)

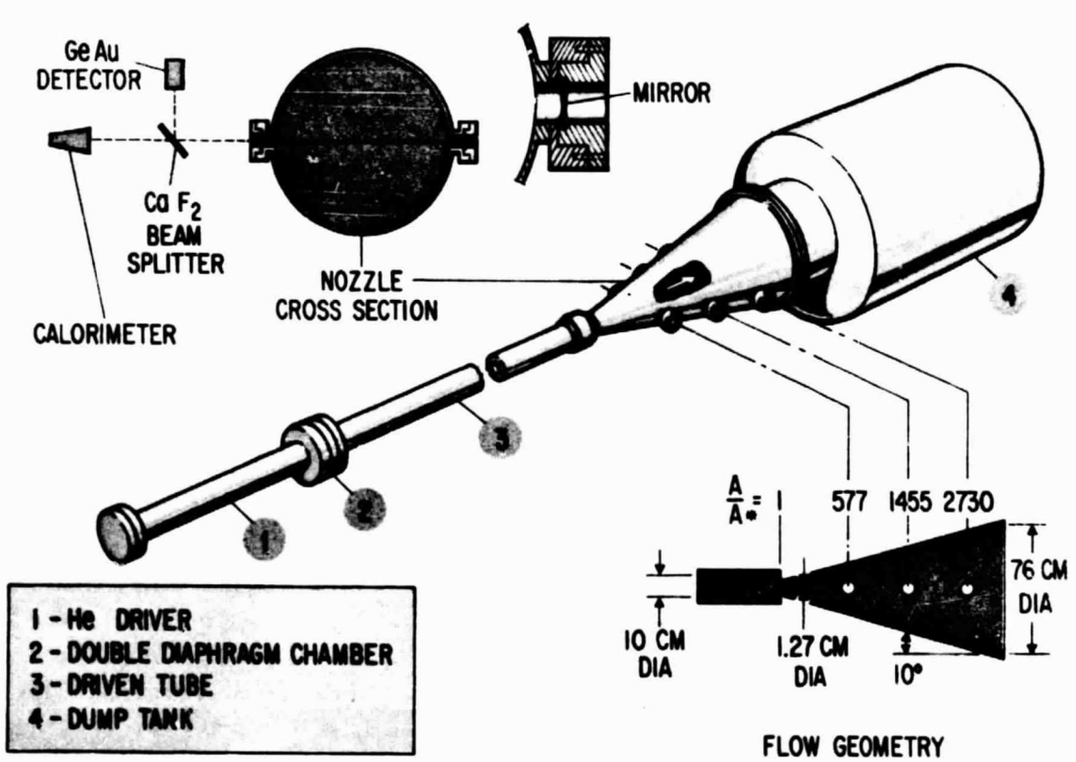

Figure 8.- Shock tunnel and instrumentation arrangement.

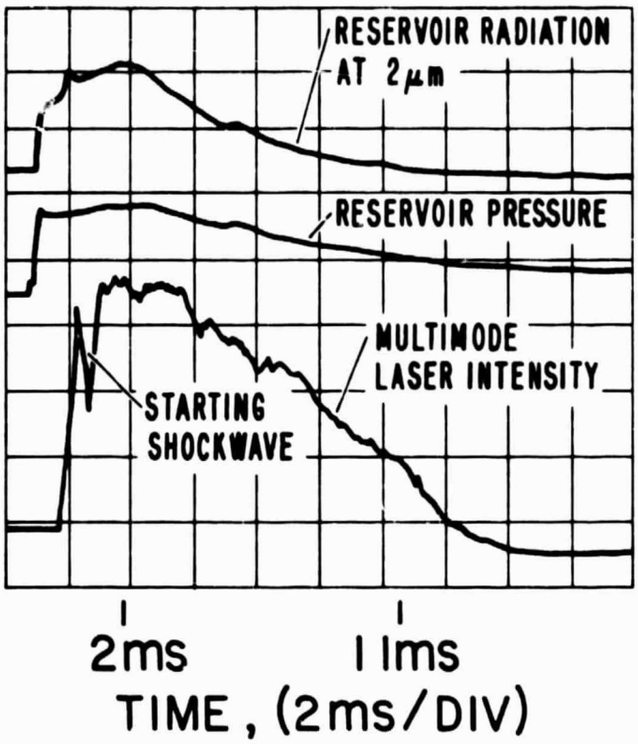

(a) 25-percent CO—75-percent N_2, T_o = 1800° K, P_o = 100 atm.

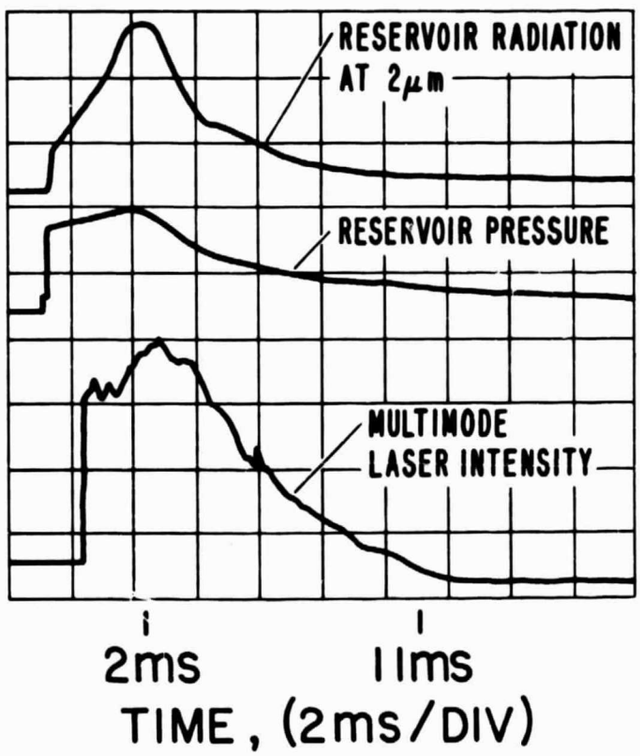

(b) 5-percent CO—15-percent N_2—80-percent Ar, T_o = 2100° K, P_o = 100 atm.

Figure 9.- Reservoir and laser intensity instrumentation records at A/A_* = 2730.

NATIONAL AERONAUTICS AND SPACE ADMINISTRATION
AMES RESEARCH CENTER, MOFFETT FIELD, CALIFORNIA

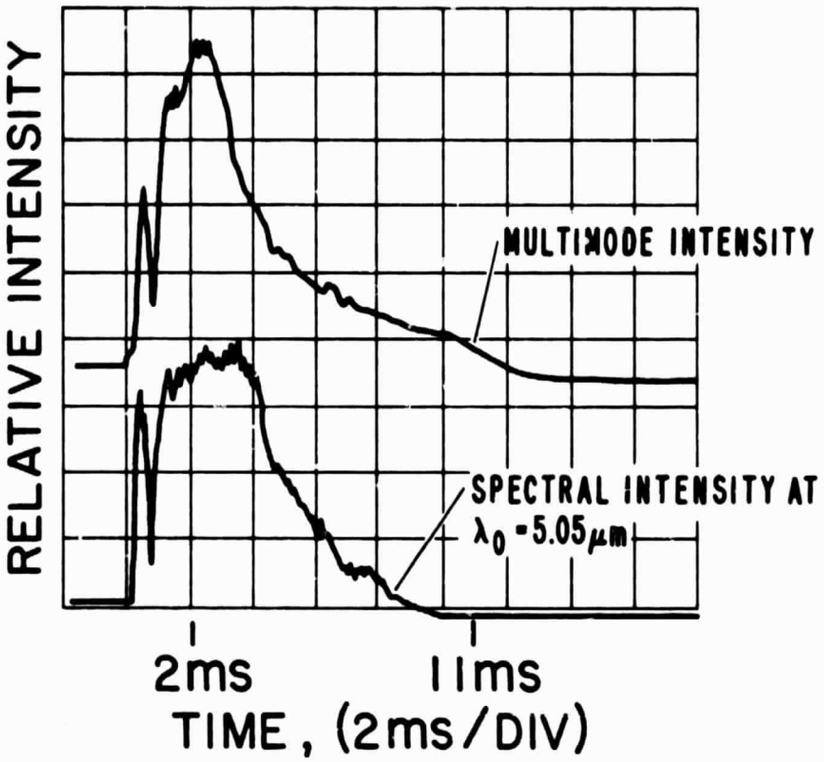

(a) λ_o = 5.05 μm

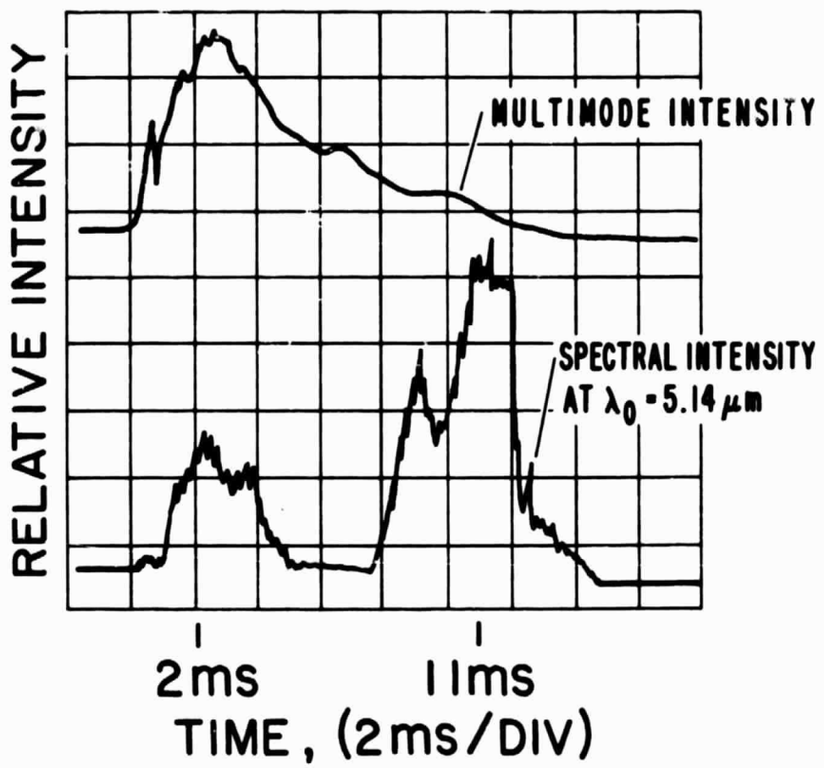

(b) λ_o = 5.14 μm

Figure 10.- Spectral and total intensity profiles from 0.25 CO - 0.75 N_2 at A/A_* = 2730, P_o = 100 atm, T_o = 1800° K. Intensity level response of the two detectors is not the same.

NATIONAL AERONAUTICS AND SPACE ADMINISTRATION
AMES RESEARCH CENTER, MOFFETT FIELD, CALIFORNIA

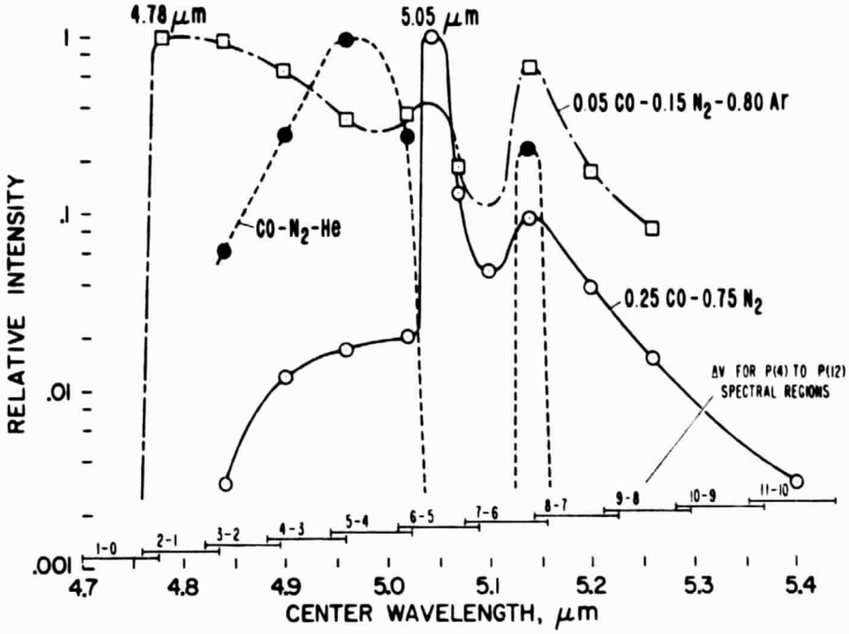

Figure 11.- Spectral characteristics at $A/A_* = 2730$. Lines connecting the data points may not indicate all spectral features.

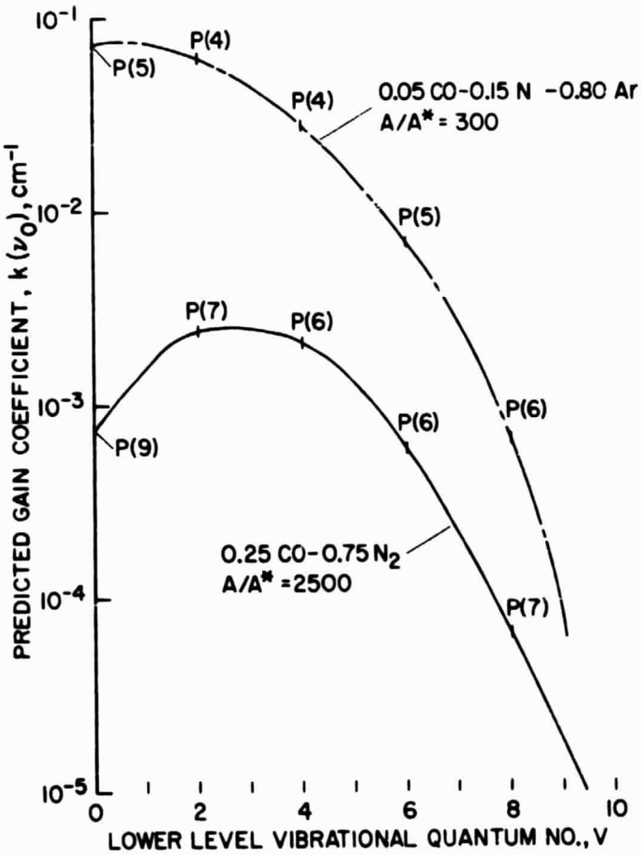

Figure 12.- Gain predictions for the experimental conditions.

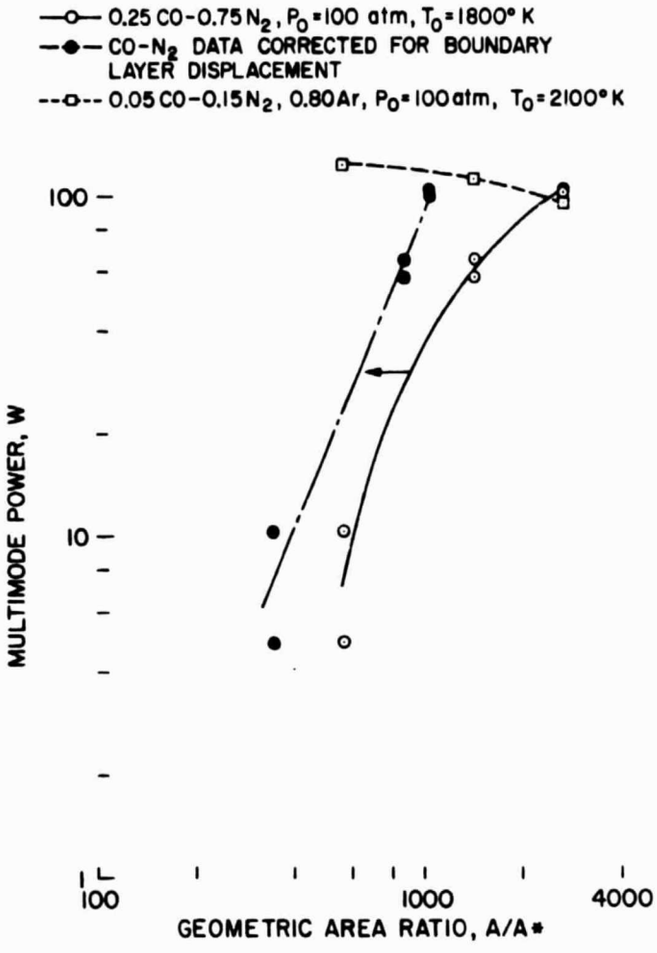

Figure 13.- Multimode power at 2 ms after starting. The boundary-layer corrections apply to the 25-percent CO - 75-percent N_2 data only. They are the result of some unpublished measurements made in N_2 flows at the same nozzle conditions by G. P. Menees.

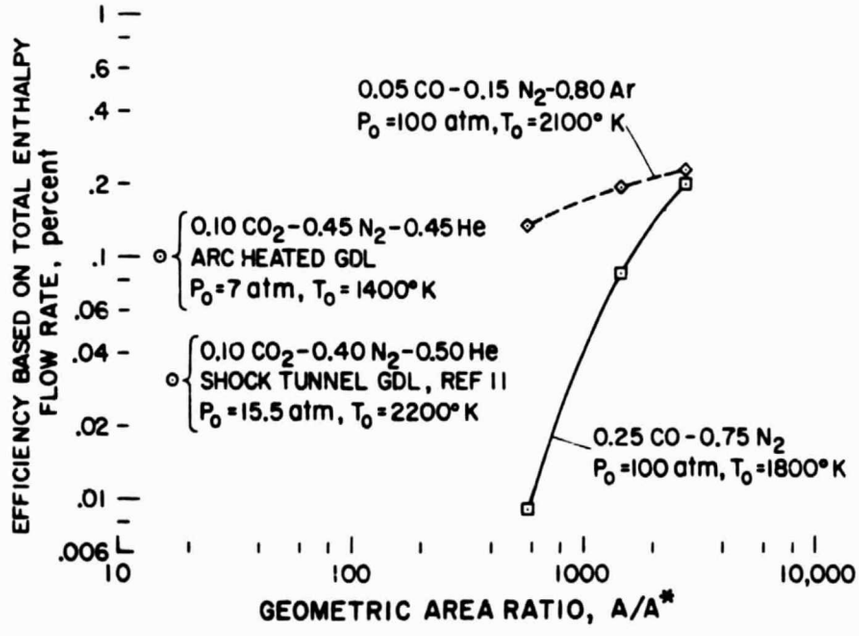

Figure 14.- Power efficiency based on equation (4). Boundary-layer corrections are not included.

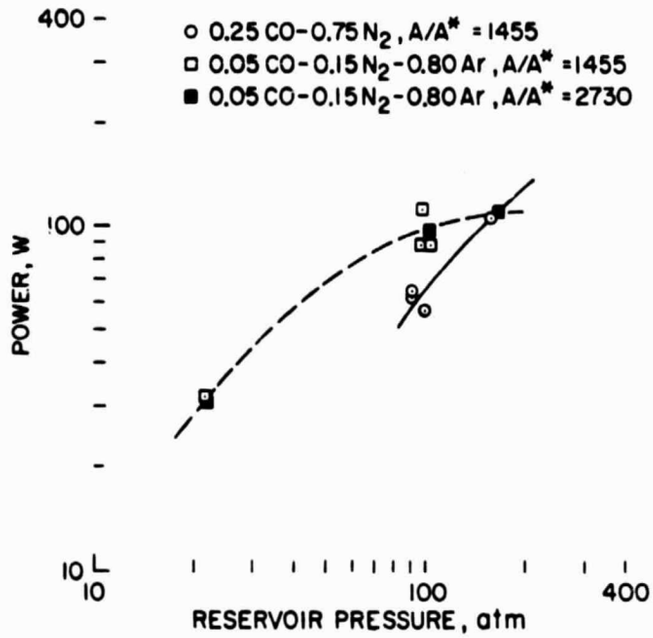

Figure 15.- The effect of reservoir pressure on multimode power at $A/A_* = 1455$ and 2730, $T_o = 1800\text{-}2100°$ K.

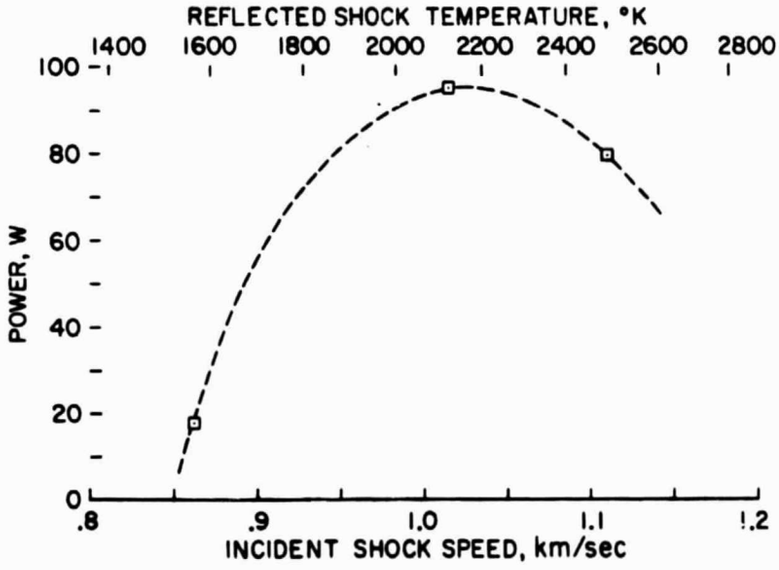

Figure 16.- The effect of reservoir temperature on multimode power for 0.05 CO - 0.15 N_2 - 0.80 Ar at $A/A_* = 2730$, $P_o = 100$ atm.